IGARSS 2024 - 2024 IEEE International Geoscience and Remote Sensing Symposium | 979-8-3503-6032-5/24/$31.00 ©2024 IEEE | DOI: 10.1109/IGARSS53475.2024.10641754

ANALYTICAL EVALUATION OF THE BASELINE DECORRELATION IN BISTATIC INTERFEROMETRIC SAR SYSTEMS

Gerardo Di Martino, Alessio Di Simone, Antonio Iodice, Daniele Riccio, Giuseppe Ruello

Dipartimento di Ingegneria Elettrica e delle Tecnologie dell'Informazione,
Università degli Studi di Napoli Federico II, 80125, Napoli, Italy
gerardo.dimartino@unina.it; alessio.disimone@unina.it; iodice@unina.it

ABSTRACT

We here analytically evaluate the spatial correlation coefficient of an interferometric pair obtained by combining two bistatic SAR acquisitions. The scattering surface is described as randomly rough, and the Kirchhoff Approximation (KA) or the first-order Small Slope Approximation (SSA1) are used to compute scattered fields. Both approximations lead to the same expression of the correlation coefficient, that generalizes to the bistatic case, with arbitrary acquisition geometry, the result available in literature for usual monostatic SAR interferometry.

Index Terms— Bistatic SAR, scattering, rough surfaces, SAR interferometry, coherence.

1. INTRODUCTION

Synthetic Aperture Radar (SAR) interferometry is a well-known technique able to retrieve accurate terrain topography [1-2] or small terrain movements [3-5] from the proper combination of multiple SAR acquisitions. The most common implementation of the technique consists in the combination of monostatic SAR images acquired at different times (repeat-pass monostatic SAR interferometry) [1-5]. The repeat-pass configuration is necessary for terrain movement retrieval, but it is often employed also for topographic applications. More accurate topography measurements are obtained by using a transmitting-and-receiving antenna and an additional receiving-only antenna (single-pass SAR interferometry) [6-7], i.e., by combining a monostatic SAR acquisition with a bistatic one. Here we will refer to this configuration as single-pass monostatic SAR interferometry.

Recently, fully bistatic implementations have been proposed [8-9] and experimentally implemented [9], that imply the use of one transmitting antenna and two closely spaced receiving-only antennas. In this case, both SAR acquisitions of the interferometric pair are bistatic, and here we will refer to this implementation as single-pass bistatic SAR interferometry. Finally, bistatic SAR experiments are being currently performed [10], thus paving the way to repeat-pass bistatic SAR interferometry, in which pairs of bistatic SAR acquisitions are used, with two transmitters, too.

In this work, we consider the general case of two closely spaced radar transmitters, and two closely spaced radar receivers placed at arbitrary distance from the transmitters. This general configuration can be easily specialized to obtain all the SAR interferometry configurations described above.

One of the main factors influencing the accuracy of interferometric measurements is coherency. The latter may be impaired by several decorrelation sources, among which baseline, or spatial, decorrelation is unavoidable, because it is caused by the fact itself that the two transmitters and/or the two receivers are spatially separated [2, 11-12]. An evaluation of the baseline decorrelation in monostatic SAR interferometry is available in [2, 11-12]. In particular, in [2, 11] it is assumed that the scattering centers belong to a flat surface and that their contribution is spatially delta-correlated, whereas in [12] the scattering surface is described as randomly rough, and the Kirchhoff Approximation (KA) is used to compute scattered fields. Results of [12] reduce to those of [2, 11] when surface correlation length is much smaller than the system resolution, as it is often the case. The approach of [12] has been recently extended to the case of one transmitter and two receivers at near-specular direction [13], which is the case of interest for Global Navigation Satellite System Reflectometry (GNSS-R), but not for SAR interferometry. A more general configuration is briefly considered in [14], where however only the single transmitter case is still considered. Here, we show how to extend the approach of [12] to the general case of two transmitters and two receivers, in order to be able to evaluate the baseline decorrelation for both single-pass and repeat-pass bistatic SAR interferometry.

2. RATIONALE

Let us consider a rough surface $z(x,y)$, whose mean plane is the x-y plane, modelled as a statistically homogeneous zero-mean Gaussian random process with standard deviation σ and normalized (to σ^2) autocorrelation function $C(\Delta x,\Delta y)$, with $\Delta x=x'-x$, $\Delta y=y'-y$, (x,y) and (x',y') being two generic surface points. The normalized autocorrelation function is equal to

one for Δx=Δy=0, and is negligible for Δx and/or Δy larger than the surface correlation length L. We assume that L is much smaller than system resolution.

The geometry of the problem is depicted in Fig. 1: we consider two identical closely spaced transmitters T1 and T2, placed at $\mathbf{r}_{T1}\equiv(x_{T1}, y_{T1}, z_{T1})$, with $x_{T1} = r_{T1}\sin\vartheta_{T1}\cos\varphi_{T1}$, $y_{T1} = r_{T1}\sin\vartheta_{T1}\sin\varphi_{T1}$, $z_{T1} = r_{T1}\cos\vartheta_{T1}$, and $\mathbf{r}_{T2}\equiv(x_{T2}, y_{T2}, z_{T2})$, with $x_{T2}=r_{T2}\sin\vartheta_{T2}\cos\varphi_{T2}$, $y_{T2}=r_{T2}\sin\vartheta_{T2}\sin\varphi_{T2}$, $z_{T2}=r_{T2}\cos\vartheta_{T2}$; and two identical closely spaced receivers R1 and R2, placed at $\mathbf{r}_{R1}\equiv(x_{R1}, y_{R1}, z_{R1})$ and $\mathbf{r}_{R2}\equiv(x_{R2}, y_{R2}, z_{R2})$, with x_{R1}, y_{R1}, z_{R1} and x_{R2}, y_{R2}, z_{R2} given by the same expressions as above, in which the subscript T is replaced by R. We also define the transmitter baseline vector $\mathbf{B}_T = \mathbf{r}_{T2} - \mathbf{r}_{T1}$ and the receiver baseline vector $\mathbf{B}_R = \mathbf{r}_{R2} - \mathbf{r}_{R1}$, and we assume that the spacing between the transmitters is much smaller than their distances from the ground ($|\mathbf{B}_T| << r_{T1}$), and similarly that the spacing between the receivers is much smaller than their distances from the ground ($|\mathbf{B}_R| << r_{R1}$), so that

$$r_{T2} - r_{T1} = B_{T\parallel}\,, \qquad \vartheta_{T2} - \vartheta_{T1} = \Delta\vartheta_T \cong \frac{B_{T\perp}}{r_{T1}}\,,$$

$$\varphi_{T2} - \varphi_{T1} = \Delta\varphi_T \cong \frac{B_{Taz}}{r_{T1}\sin\vartheta_{T1}}\,, \tag{1}$$

and identical relationships hold for the receivers, with the subscript T replaced by the subscript R. In (1), $B_{T\parallel}, B_{T\perp}, B_{Taz}$ and $B_{R\parallel}, B_{R\perp}, B_{Raz}$ are the parallel, perpendicular, and azimuth components of the baseline vectors:

$$\mathbf{B}_T = B_{T\parallel}\hat{\mathbf{r}}_{T1} + B_{T\perp}\hat{\boldsymbol{\vartheta}}_{T1} + B_{Taz}\,\hat{\boldsymbol{\varphi}}_{T1}\,,$$
$$\mathbf{B}_R = B_{R\parallel}\hat{\mathbf{r}}_{R1} + B_{R\perp}\hat{\boldsymbol{\vartheta}}_{R1} + B_{Raz}\,\hat{\boldsymbol{\varphi}}_{R1}\,. \tag{2}$$

The origin O of the reference system coincides with the center of the considered resolution cell. We assume perfect co-registration of the image pair, so that the center of the resolution cell is the same for both images.

By using the KA, the generic component of the field $E_1(\mathbf{r}_{R1})$ transmitted by T1 and scattered towards R1 can be written as

$$E_1(\mathbf{r}_{R1}) = \int_{-\infty}^{\infty}\int_{-\infty}^{\infty} F_1(x,y)w(x,y)\frac{\exp\{-jk[\tilde{R}_{T1}(x,y)+\tilde{R}_{R1}(x,y)]\}}{\tilde{R}_{T1}(x,y)\tilde{R}_{R1}(x,y)}dxdy\,. \tag{3}$$

Similarly, the generic component of the field $E_2(\mathbf{r}_{R2})$ transmitted by T2 and scattered towards R2 can be written as

$$E_2(\mathbf{r}_{R2}) = \int_{-\infty}^{\infty}\int_{-\infty}^{\infty} F_2(x,y)w(x,y)\frac{\exp\{-jk[\tilde{R}_{T2}(x,y)+\tilde{R}_{R2}(x,y)]\}}{\tilde{R}_{T2}(x,y)\tilde{R}_{R2}(x,y)}dxdy\,. \tag{4}$$

In (3-4) $k=2\pi/\lambda$ is the wavenumber, with λ being the wavelength, $F_{1,2}(x,y)$ are slowly-varying functions, proportional to the incident field, whose expressions, as shown in the following, are of no interest here, and $w(x,y)$ is the sensor illumination function, whose shape may be irregular, depending on the observation geometry and on the platforms' flight directions. We will consider the case of arbitrary illumination function, assuming that its x and y sizes (i.e., the sensors' x and y resolutions) are A_x and A_y, respectively, but we will also specialize the obtained expressions in the Gaussian case:

$$w(x,y) = \exp\left(-\frac{x^2}{2A_x^2} - \frac{y^2}{2A_y^2}\right)\,. \tag{5}$$

In addition, in (4)

$$\tilde{R}_X(x,y) = \sqrt{(z_X - z)^2 + (x_X - x)^2 + (y_X - y)^2} = R_X(x,y)\sqrt{1 + \frac{z^2 - 2z_X z}{R_X^2(x,y)}} \cong \cong R_X(x,y) - \frac{z_X}{R_X(x,y)}z(x,y) \tag{6}$$

with $R_X(x,y) = \sqrt{z_X^2 + (x_X - x)^2 + (y_X - y)^2}$, (7)

and with the subscript X that must be replaced by $T1$, $T2$, $R1$ or $R2$ as needed, so that, while r_X are the distances of sensors from the origin, R_X are their distances from the generic point $(x,y,0)$ of the mean plane, and $\tilde{R}_X$ are their distances from the generic point $(x,y,z(x,y))$ of the rough surface.

We explicitly note that the same formulation (3-4) also holds under the first-order Small-Slope Approximation (SSA1) [15], with different expressions of $F_{1,2}(x,y)$. This ensures that our results for the correlation coefficient are valid under both the KA and the SSA1.

We want now to compute the correlation coefficient

$$\rho = \frac{|\mathrm{cov}[E_1(\mathbf{r}_{R1})E_2(\mathbf{r}_{R2})]|}{\sqrt{\mathrm{var}[E_1(\mathbf{r}_{R1})]\mathrm{var}[E_2(\mathbf{r}_{R2})]}}\,, \tag{8}$$

where

$$\mathrm{cov}[E_1(\mathbf{r}_{R1})E_2(\mathbf{r}_{R2})] = \langle[E_1(\mathbf{r}_{R1}) - \langle E_1(\mathbf{r}_{R1})\rangle][E_2(\mathbf{r}_{R2}) - \langle E_2(\mathbf{r}_{R2})\rangle]^*\rangle = \langle E_1(\mathbf{r}_{R1})E_2(\mathbf{r}_{R2})^*\rangle - \langle E_1(\mathbf{r}_{R1})\rangle\langle E_2(\mathbf{r}_{R2})\rangle^*\,, \tag{9}$$

$$\mathrm{var}\left[E_{1,2}(\mathbf{r}_{R1,2})\right] = \langle\left|E_{1,2}(\mathbf{r}_{R1,2}) - \langle E_{1,2}(\mathbf{r}_{R1,2})\rangle\right|^2\rangle = \langle\left|E_{1,2}(\mathbf{r}_{R1,2})\right|^2\rangle - \left|\langle E_{1,2}(\mathbf{r}_{R1,2})\rangle\right|^2\,, \tag{10}$$

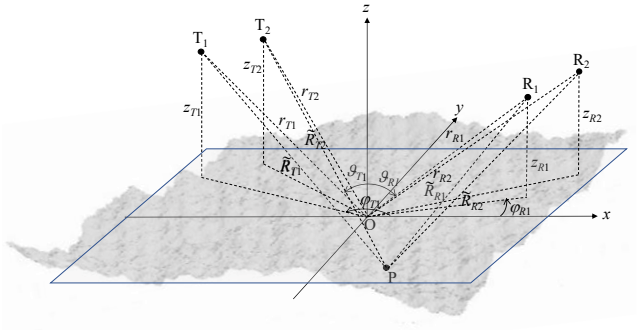

Figure 1: Geometry of the problem.

and the symbol $\langle\cdot\rangle$ indicates the statistical mean.

By using (3-4) in (9) and by employing the same approach of [13], we get

$$\begin{aligned}&\mathrm{cov}[E_1(\mathbf{r}_{R1})E_2(\mathbf{r}_{R2})] \cong \\ &\cong \int_{-\infty}^{\infty}\int_{-\infty}^{\infty}\frac{F_1(x,y)F_2^*(x,y)w^2(x,y)}{R_{T1}(x,y)R_{T2}(x,y)R_{R1}(x,y)R_{R2}(x,y)} \\ &\exp\{-jk[R_{T1}(x,y)-R_{T2}(x,y)+R_{R1}(x,y)- \\ &R_{R2}(x,y)]\}\exp\left\{-\frac{k^2\sigma^2}{2}[u_{z1}(x,y)-u_{z2}(x,y)]^2\right\} \\ &\tilde{F}\left(x,y,ku_x(x,y),ku_y(x,y)\right)dxdy \quad , \end{aligned} \tag{11}$$

where

$$\begin{aligned}u_x(x,y)&=\frac{\partial(R_{T1}+R_{R1})}{\partial x}=\frac{x-x_{T1}}{R_{T1}(x,y)}+\frac{x-x_{R1}}{R_{R1}(x,y)} \quad , \\ u_y(x,y)&=\frac{\partial(R_{T1}+R_{R1})}{\partial y}=\frac{y-y_{T1}}{R_{T1}(x,y)}+\frac{y-y_{R1}}{R_{R1}(x,y)} \quad , \\ u_{z1,2}(x,y)&=\frac{z_{T1,2}}{R_{T1,2}(x,y)}+\frac{z_{R1,2}}{R_{R1,2}(x,y)} \quad ,\end{aligned} \tag{12}$$

and $\tilde{F}$ is the Fourier Transform, with respect to Δx and Δy, of

$$\begin{aligned}&\tilde{f}(x,y,\Delta x,\Delta y)= \\ &=\exp\{-k^2\sigma^2u_{z1}(x,y)u_{z2}(x,y)[1-C(\Delta x,\Delta y)]\}- \\ &\exp\{-k^2\sigma^2u_{z1}(x,y)u_{z2}(x,y)\} \quad .\end{aligned} \tag{13}$$

Note that $\tilde{F}$ is real, due to the symmetry properties of the autocorrelation function.

The sensor illumination function w in (11) is peaked around the origin and is appreciably different from zero only in the resolution cell of area of the order of A_xA_y. Since the resolution is usually much smaller than r_{T1} and r_{R1}, in the resolution cell the argument of the first exponential in (11) can be approximated by expanding it around the origin:

$$\begin{aligned}&R_{T1}(x,y)-R_{T2}(x,y)+R_{R1}(x,y)-R_{R2}(x,y)\cong r_{T1}- \\ &r_{T2}+r_{R1}-r_{R2}+\eta_x x+\eta_y y \quad ,\end{aligned} \tag{14}$$

where $\eta_x=\eta_{Tx}+\eta_{Rx}$ and $\eta_y=\eta_{Ty}+\eta_{Ry}$ with

$$\begin{aligned}\eta_{Tx}&=\frac{\partial(R_{T1}-R_{T2})}{\partial x}\Big|_{\substack{x=0\\y=0}}=-\frac{x_{T1}}{r_{T1}}+\frac{x_{T2}}{r_{T2}}= \\ &=-\sin\vartheta_{T1}\cos\varphi_{T1}+\sin\vartheta_{T2}\cos\varphi_{T2}\cong\cos\vartheta_{T1}\cos\varphi_{T1}\Delta\vartheta_T- \\ &\sin\vartheta_{T1}\sin\varphi_{T1}\Delta\varphi_T\cong\frac{\cos\vartheta_{T1}\cos\varphi_{T1}B_{T\perp}}{r_{T1}}-\frac{\sin\varphi_{T1}B_{Taz}}{r_{T1}} \\ \eta_{Ty}&=\frac{\partial(R_{T1}-R_{T2})}{\partial y}\Big|_{\substack{x=0\\y=0}}=-\frac{y_{T1}}{r_{T1}}+\frac{y_{T2}}{r_{T2}}= \\ &=-\sin\vartheta_{T1}\sin\varphi_{T1}+\sin\vartheta_{T2}\sin\varphi_{T2}\cong\cos\vartheta_{T1}\sin\varphi_{T1}\Delta\vartheta_T+ \\ &\sin\vartheta_{T1}\cos\varphi_{T1}\Delta\varphi_T\cong\frac{\cos\vartheta_{T1}\sin\varphi_{T1}B_{T\perp}}{r_{T1}}+\frac{\cos\varphi_{T1}B_{Taz}}{r_{T1}} \quad ,\end{aligned} \tag{15}$$

η_{Rx} and η_{Ry} being obtained from (15) by replacing the subscript $T1$ and $T2$ with $R1$ and $R2$, respectively.

All other functions in (11) can be assumed approximately constant in the resolution cell and equal to their value in the origin:

$$F_{1,2}(x,y)\cong F_{1,2}(0,0)=F_{10,20}\,, \tag{16}$$

$$\begin{aligned}&u_{z1}(x,y)-u_{z2}(x,y)\cong u_{z1}(0,0)-u_{z2}(0,0)=\cos\vartheta_{T1}+ \\ &\cos\vartheta_{R1}-\cos\vartheta_{T2}-\cos\vartheta_{R2}\cong\sin\vartheta_{T1}\Delta\vartheta_T+\sin\vartheta_{R1}\Delta\vartheta_R\cong \\ &\cong\frac{\sin\vartheta_{T1}B_{T\perp}}{r_{T1}}+\frac{\sin\vartheta_{R1}B_{R\perp}}{r_{R1}} \quad ,\end{aligned} \tag{17}$$

$$\tilde{F}\cong\tilde{F}\left(0,0,ku_x(0,0),ku_y(0,0)\right)=\tilde{F}_0\,. \tag{18}$$

By using (14) and (16-18) in (11) we get

$$\begin{aligned}&\mathrm{cov}[E_1(\mathbf{r}_{R1})E_2(\mathbf{r}_{R2})]\cong\frac{F_{10}F_{20}^*\tilde{F}_0\exp[-jk(r_{T1}-r_{T2}+r_{R1}-r_{R2})]}{r_{T1}r_{T2}r_{R1}r_{R2}} \\ &\exp\left\{-\frac{k^2\sigma^2}{2}\left[\frac{\sin\vartheta_{T1}B_{T\perp}}{r_{T1}}+\frac{\sin\vartheta_{R1}B_{R\perp}}{r_{R1}}\right]^2\right\} \\ &\int_{-\infty}^{\infty}\int_{-\infty}^{\infty}w^2(x,y)\exp\left[-jk\eta_x x-jk\eta_y y\right]dxdy \quad .\end{aligned} \tag{19}$$

The double integral over x and y in (19) is the FT of $w^2(x,y)$ evaluated in $k\eta_x$, $k\eta_y$, so that we can write, by using also (15):

$$\begin{aligned}&\mathrm{cov}[E_1(\mathbf{r}_{R1})E_2(\mathbf{r}_{R2})]=\frac{F_{10}F_{20}^*\tilde{F}_0\exp[jk(B_{T\parallel}+B_{R\parallel})]}{r_{T1}r_{T2}r_{R1}r_{R2}} \\ &\exp\left\{-\frac{k^2\sigma^2}{2}\left[\frac{\sin\vartheta_{T1}B_{T\perp}}{r_{T1}}+\frac{\sin\vartheta_{R1}B_{R\perp}}{r_{R1}}\right]^2\right\} \\ &\mathrm{W}_{sq}\left\{k\left[\frac{\cos\vartheta_{T1}\cos\varphi_{T1}B_{T\perp}}{r_{T1}}-\frac{\sin\varphi_{T1}B_{Taz}}{r_{T1}}+\frac{\cos\vartheta_{R1}\cos\varphi_{R1}B_{R\perp}}{r_{R1}}-\right.\right. \\ &\left.\frac{\sin\varphi_{R1}B_{Raz}}{r_{R1}}\right],k\left[\frac{\cos\vartheta_{T1}\sin\varphi_{T1}B_{T\perp}}{r_{T1}}+\frac{\cos\varphi_{T1}B_{Taz}}{r_{T1}}+ \\ &\left.\left.\frac{\cos\vartheta_{R1}\sin\varphi_{R1}B_{R\perp}}{r_{R1}}+\frac{\cos\varphi_{R1}B_{Raz}}{r_{R1}}\right]\right\} \quad ,\end{aligned} \tag{20}$$

where $\mathrm{W}_{sq}(k\eta_x,k\eta_y)$ is the FT of $w^2(x,y)$.

The field variances are easily deduced from (20) by setting all baselines to zero.

By replacing (20) and field variances in (8), we finally get

$$\begin{aligned}&\rho\cong\exp\left\{-\frac{k^2\sigma^2}{2}\left[\frac{\sin\vartheta_{T1}B_{T\perp}}{r_{T1}}+\frac{\sin\vartheta_{R1}B_{R\perp}}{r_{R1}}\right]^2\right\} \\ &\left|\mathrm{W}_{sq}\left\{k\left[\frac{\cos\vartheta_{T1}\cos\varphi_{T1}B_{T\perp}}{r_{T1}}-\frac{\sin\varphi_{T1}B_{Taz}}{r_{T1}}+\frac{\cos\vartheta_{R1}\cos\varphi_{R1}B_{R\perp}}{r_{R1}}-\right.\right.\right. \\ &\left.\frac{\sin\varphi_{R1}B_{Raz}}{r_{R1}}\right],k\left[\frac{\cos\vartheta_{T1}\sin\varphi_{T1}B_{T\perp}}{r_{T1}}+\frac{\cos\varphi_{T1}B_{Taz}}{r_{T1}}+ \\ &\left.\left.\left.\frac{\cos\vartheta_{R1}\sin\varphi_{R1}B_{R\perp}}{r_{R1}}+\frac{\cos\varphi_{R1}B_{Raz}}{r_{R1}}\right]\right\}/\mathrm{W}_{sq}(0,0)\right| \quad .\end{aligned} \tag{21}$$

By using a well-known property of the FT, i.e., the uncertainty principle, we can state that $\mathrm{W}_{sq}(k\eta_x,k\eta_y)$ is appreciably different from zero only if $k\eta_x$ is not larger than a critical value of the order of $1/A_x$ and if, at the same time, $k\eta_y$ is not larger than a critical value of the order of $1/A_y$. For instance, if the Gaussian illumination function of (5) is considered, we get

$$\mathrm{W}_{sq}(k\eta_x,k\eta_y)=\pi A_xA_y\exp\left\{-\frac{k^2\eta_x^2A_x^2}{4}-\frac{k^2\eta_y^2A_y^2}{4}\right\} \quad , \tag{22}$$

and the critical values for $k\eta_x$ and $k\eta_y$ are $2/A_x$ and $2/A_y$, respectively.

Equations (21-22) allow us to compute the correlation coefficient for a very general bistatic geometry, and it can be verified that they reduce to the available ones in the monostatic case.

3. NUMERICAL RESULTS

We here illustrate a numerical example by considering a backward scattering coplanar geometry, i.e., see Fig. 2, $\varphi_{R1} = \varphi_{T1}$. In addition, we assume $B_{Raz} = B_{Taz} = 0$, $r_{R1} = r_{T1} = 800$ km , $A_x = A_y = 5$ m , $B_{T\perp} = 400$ m , and $\vartheta_{T1} = 30°$, and show the plots of ρ vs. $B_{R\perp}$ for different values of ϑ_{R1} in Fig. 3. Note that, in this coplanar geometry, it is possible to obtain a unitary correlation coefficient with non-null orthogonal baselines. In fact, it is sufficient that

$$\frac{\cos\vartheta_{T1}B_{T\perp}}{r_{T1}} = -\frac{\cos\vartheta_{R1}B_{R\perp}}{r_{R1}} \quad . \tag{23}$$

It can be verified that under this condition we also have that the phase sensitivity to topography is null.

4. CONCLUSION

A closed-form expression of the spatial correlation coefficient has been provided for a very general bistatic SAR interferometric geometry. Numerical examples have been presented.

5. ACKNOWLEDGMENT

This work was supported by the Italian Space Agency through the Project "SimulAzione e Modellazione del Sistema BistAtico COSMO-SkyMed/Platino (SAMBA)".

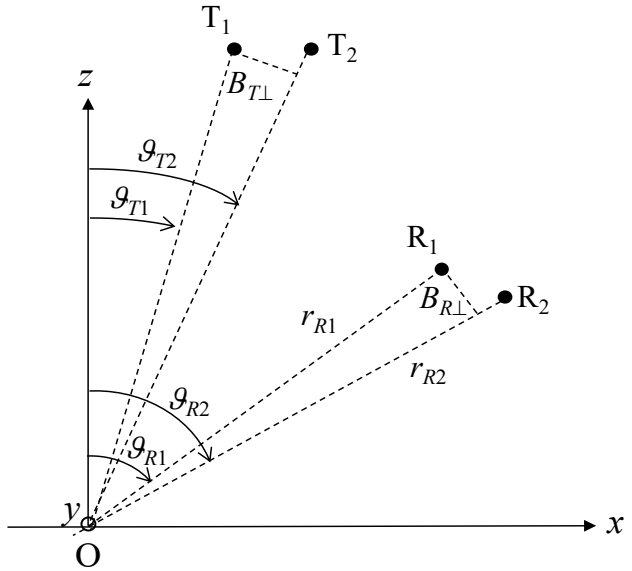

Figure 2: Backward scattering coplanar geometry.

6. REFERENCES

[1] H. A. Zebker and R. M. Goldstein, "Topographic mapping from interferometric synthetic aperture radar observations", *J. Geophys. Res.*, vol. 91, no. B5, pp. 4993-4999, Apr. 1986.

[2] E. Rodriguez and J. M. Martin, "Theory and design of interferometric synthetic aperture radars", *IEE Proc. F*, vol. 139, no. 23, pp. 147-159, Apr. 1992.

[3] A. K. Gabriel, R. M. Goldstein, and H. A. Zebker, "Mapping small elevation changes over large areas: Differential interferometry", *J. Geophys. Res.,* vol.94, pp. 9183-9191, 1989.

[4] Ferretti, A., Prati, C., Rocca, F., "Permanent scatterers in SAR interferometry", *IEEE Trans. Geosci. Remote Sens.*, Vol. 39, No.1, pp. 8-20, 2001.

[5] Berardino, P., Fornaro, G., Lanari, R., Sansosti, E., "A new algorithm for surface deformation monitoring based on small baseline differential SAR interferograms", *IEEE Trans. Geosci. Remote Sens.*, Vol. 40, No.11, pp. 2375-2383, 2002.

[6] R. Bamler, "The SRTM mission: A world-wide 30 m resolution DEM from SAR interferometry in 11 days," in *Photogrammetric Week*, R. Fritsch and R. Spiller, Eds, 1999, pp. 145–154.

[7] M. Zink *et al*., "TanDEM-X: 10 Years of Formation Flying Bistatic SAR Interferometry," *IEEE J. Sel. Topics Appl. Earth Observ. Remote Sens.*, vol. 14, pp. 3546-3565, 2021.

[8] P. López-Dekker *et al*., "Companion SAR constellations for single-pass interferometric applications: The SESAME mission," *IGARSS 2017*, Fort Worth, TX, USA, 2017, pp. 119-122.

[9] S. Duque, P. Lopez-Dekker and J. J. Mallorqui, "Single-Pass Bistatic SAR Interferometry Using Fixed-Receiver Configurations: Theory and Experimental Validation," *IEEE Trans. Geosci. Remote Sens.*, vol. 48, no. 6, pp. 2740-2749, June 2010.

[10] G. Farquharson *et al*., "The New Capella Space Satellite Generation: Acadia," *IGARSS 2023*, Pasadena, CA, USA, 2023, pp. 1513-1516.

[11] H. A. Zebker and J. Villasenor, "Decorrelation in interferometric radar echoes," *IEEE Trans. Geosci. Remote Sens.*, vol. 30, no. 5, pp. 950-959, Sep. 1992.

[12] G. Franceschetti, A. Iodice, M. Migliaccio, and D. Riccio, "The effect of surface scattering on IFSAR baseline decorrelation," *J. Electrom. Waves Applications*, vol. 11, no. 3, pp. 353-370, 1997.

[13] G. D. Martino, A. Di Simone, and A. Iodice, "An Analytical Formulation of the Correlation of GNSS-R Signals," *IEEE Trans. Geosci. Remote Sens.*, vol. 60, Art no. 2005913, pp. 1-13, 2022.

[14] G. Di Martino, A. Di Simone, and A. Iodice, "An Analytical Formulation for the Correlation of Surface-Scattered Fields at Two Bistatic Radar Receivers," *IGARSS 2022*, Kuala Lumpur, Malaysia, 2022, pp. 4969-4972.

[15] A. G. Voronovich, "Small-slope approximation for electromagnetic wave scattering at a rough interface of two dielectric half-spaces," *Waves Random Media*, vol. 4, pp. 337–367, 1994.

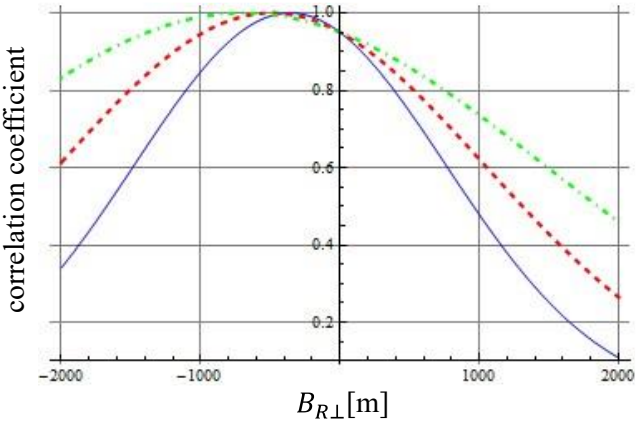

Figure 3: Correlation coefficient ρ vs. orthogonal baseline of the receiving antennas $B_{R\perp}$, for ϑ_{R1}=15° (blue), 45° (red), and 60° (green). The values of all other parameters are defined in Section 3.